Infrared Physics & Technology, Volume 125, September 2022, Article number 104277
DOI:10.1016/j.infrared.2022.104277

Non-destructive imaging of marqueteries based on a new infrared-terahertz fusion technique

Jue Hu[a,c], Hai Zhang[b,c,*], Stefano Sfarra[d], Gianfranco Gargiulo[e], Nicolas P. Avdelidis[c,f], Mingli Zhang[g], Dazhi Yang[h], Xavier Maldague[c]

[a] *School of Automation Engineering, University of Electronic Science and Technology of China, Chengdu 611731, China*
[b] *Centre for Composite Materials and Structures (CCMS), Harbin Institute of Technology, Harbin 150001, China*
[c] *Computer Vision and Systems Laboratory (CVSL), Department of Electrical and Computer Engineering, Laval University, Quebec G1V 0A6, Canada*
[d] *Department of Industrial and Information Engineering and Economics, University of L'Aquila, 67100 L'Aquila, Italy*
[e] *Individual Company of Restoration, 80073 Capri, Italy*
[f] *School of Aerospace, Transport and Manufacturing, Cranfield University, Cranfield MK43 0AL, UK*
[g] *McGill Centre for Integrative Neuroscience, Montreal Neurological Institute, McGill University, Montreal H3A 2B4, Canada*
[h] *School of Electrical Engineering and Automation, Harbin Institute of Technology, Harbin, Heilongjiang, China*
** Corresponding author: hai.zhang.1@ulaval.ca (Hai Zhang)*

Abstract: Detection of subsurface defects has hitherto been regarded as an important element in the course of preserving cultural heritage. To do so, non-invasive imaging approaches for viewing and determining the location of splitting inside the sample under test are required, which constitute the subject of the present study. Both active thermography and terahertz imaging have demonstrated their potential in providing non-destructive inspection on cultural heritage objects. Conventionally, active thermography has been used to retrieve details on the defects as well as morphological data from the surface and subsurface, whereas pulsed terahertz imaging has been applied to record the internal material distribution. Here, the feature extraction, selection and fusion framework is extended to design a fusion process to merge the information obtained by both active thermography and terahertz imaging; in this way, the technique naturally inherits the strengths of both aforementioned imaging technologies. The fusion technique is able to produce images with high-contrast defect information located at different depths. To demonstrate the efficacy of the suggested technique, an experiment has been conducted on an ancient marquetry.

Keywords: cultural heritage, infrared thermography, terahertz imaging, data fusion.

Published by Elsevier. This is the Author Accepted Manuscript issued with: Creative Commons Attribution Non-Commercial No Derivatives License (CC:BY:NC:ND 4.0).
The final published version (version of record) is available online at DOI:10.1016/j.infrared.2022.104277. Please refer to any applicable publisher terms of use.

1 Introduction

There has been a growing interest in the preservation and conservation of cultural heritage artifacts [1]–[3]. Applications of scientific methods in the field of non-destructive inspection (NDI) of cultural heritage are continuously expanding. Subsurface defects, in particular, have the potential to cause significant harm to the cultural heritage that needs to be preserved. In this regard, an imaging approach, as to view and thus determine the location of splitting inside the sample under test, is required. During the inspection of artworks, a variety of imaging techniques have been utilized, including ultraviolet fluorescence [4], [5], acoustic imaging [6], X-ray [7], infrared thermography [8], among other approaches. Fluorescence imaging is a technique for determining the state of paint surfaces and varnish layers. This method, which creates a 2D representation of surface paint layers, is able to detect ultraviolet-absorbing fluorescent-emitting substances, which suggest possible retouching or old varnish layers. The acoustic method is usually used by conservators for defect detection in frescoes. However, as this method yields only approximate results, only experts are able to determine the severity of the defect accurately. High-resolution diagnostics of a wide range of artworks, including mural paintings, sculptures, and monuments, are possible with portable X-ray tubes and digital X-ray detectors. That said, X-ray pictures are frequently affected by the superposition of other images due to the thickness of the material, resulting in undesirable consequences.

Among the most relevant NDI methods, active thermography [9]–[11] and terahertz imaging [12]–[14] are of the highest significance, and several studies have already demonstrated their utility in examining cultural heritage objects of disparate structures and materials. By controlling the intensity of the external energy source, active thermography can provide information concerning the surface of cultural heritage as well as their thermal properties [15]–[18]. Because active thermography produces data with a high signal-to-noise ratio (SNR), it is routinely employed to investigate the thermal characteristics of the sample of concern. Mercuri et al. [19], for instance, studied a painted altarpiece preserved inside the Basilica of Santa Maria in Cosmedin, Rome, Italy, by combining three imaging techniques operating in the near- and mid-infrared spectral ranges. The results enabled the detection of damage in the wooden support and the identification of pictorial features buried beneath the visible paint layer, thus providing valuable information. Tavakolian et al. [20] proposed an infrared tomography method for wood inlay inspection. Chirped laser beam was used as a modulated excitation source for heat generation, while the thermal sequence was recorded with a mid-infrared camera and processed by a cross-correlation algorithm, as to obtain infrared images in a layer-by-layer modality. Defects such as empty holes or subsurface splitting of the wood inlay specimen were identified with this method. Yao et al. [21] conducted a comparative study on a *Madonna* panel painting, which has four fabricated defects. Three thermal data processing methods including pixel-wise algorithm for time-derivative of temperature, independent component thermography

and sparse principal component thermography were compared so as to identify the most suitable method in terms of contrast enhancement on the defective regions. The results showed that independent component thermography method effectively improved the contrast at the end of the procedure.

Terahertz radiation can be used to investigate cultural heritage artifacts in a non-contact and non-destructive fashion [22]. In a variety of materials, such as plaster, wood, or ceramics, it has demonstrated to have a significant penetration depth, providing internal information concerning the realization of cultural heritage objects. Groves et al. [23] investigated into the pulsed terahertz imaging technique for structural diagnostics of wooden panel paintings. Amplitude and time-delay features were both proved to be effective in revealing cracks on the wooden support. Dong et al. [24] leveraged the terahertz reflective imaging approach for diagnosis of a mid-20th century Italian painting titled *After Fishing*. Frequency-wavelet domain deconvolution (FWDD) was applied to obtain the impulse response function of the terahertz reflection signals. Stratigraphic imaging was achieved by calculating the absolute value of the reflective peaks. It is worth noting that terahertz reflective imaging using FWDD signals is able to disclose spots in the paperboard that are not identifiable through X-ray techniques.

Based on the above discussion, it is possible to say that, no sensor or measuring system is able to provide adequate information for the structural diagnosis of cultural heritage objects [25]. In order to fully exploit the features provided by detection systems such as active thermography and terahertz imaging, a data fusion approach is implemented in this work. An ancient marquetry is used as the object under study.

Firstly, feature extraction, selection and fusion (FE-S-F), as a data fusion framework, is applied to data from two active thermography techniques; in this way, the features extracted from different excitation modes and at different depths can be combined together [26].

Subsequently, the FE-S-F framework is extended to extract, select and fuse features from active thermography and terahertz imaging. On the one hand, the active thermography is able to reveal the details of defects as well as the morphological information from both the surface and subsurface. On the other hand, the terahertz imaging can record material distribution at different depths.

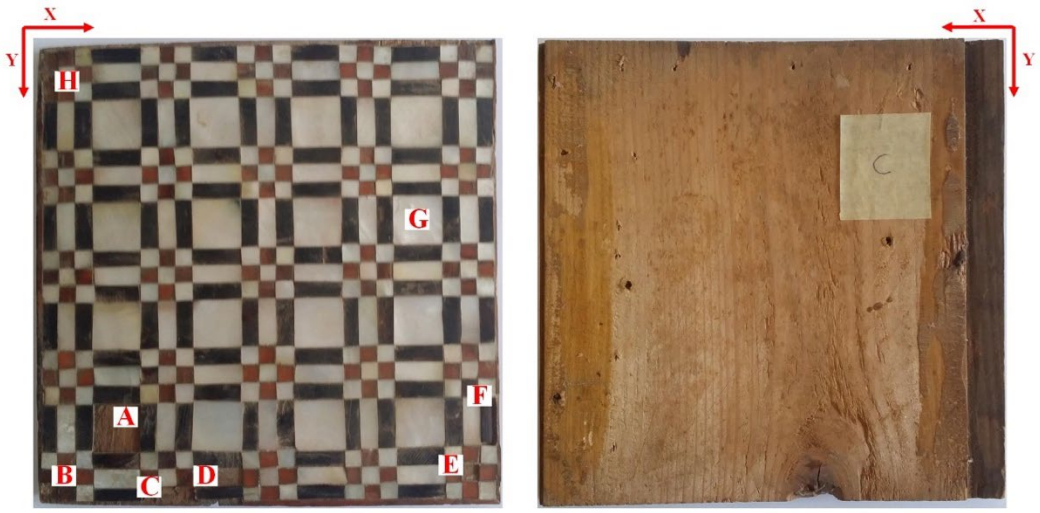
Generally, the feature extraction stage collects features, which, in this case, include time-domain, frequency-domain, and statistical ones. Feature selection based on the SNR of the defect region is carried out next, as to select suitable feature images for the fusion stage. Finally, the fused results are generated via an unsupervised deep residual fusion network based on fusing feature images from two excitation modalities; the latter is found to be able to intuitively depict both surface and sub-surface defects.

2 Material and method

2.1 Marquetry sample

The ancient marquetry of concern, as shown in Fig. 1, consists of three layers. The support is made of fir wood, the middle is the animal glue, and the top is the ornamental layer, which is a composite of several materials, including but not limited

to pearl (white tesserae) and bovine horn [27]. The perimeter is built using boxwood. Seven obvious defects (i.e., missing and broken tesserae) can be identified through just visual inspection, as marked in Fig. 1(a). The defect G, unlike others, is not conspicuous, as it refers to a detachment region, which has been initially identified by a tap test. In addition, decays due to microbiological growth and moisture can be seen on the rear side of the sample (see Fig. 1b).



(a) (b)

Fig. 1. Photographs of the ancient marquetry: (a) front side, and (b) rear side.

2.2 Infrared-terahertz fusion imaging

The active thermography data are collected with a dynamic line-scan technique under the experimental setup of Fig. 2. The setup is composed of a line heat source and a longwave infrared camera (FLIR Phoenix, NETD = 50 mK). The data sampling rate is regulated as to guarantee that data processing can be done concurrently with scanning, owed to the need for dynamic analysis of the *in-situ* inspection data. The infrared camera has a spatial resolution of 640 × 512 pixels and a sampling rate of 55 frames per second (fps). The marquetry sample is fixed and manipulated to go through the lined heat source by *x*-*y* scanning platform.

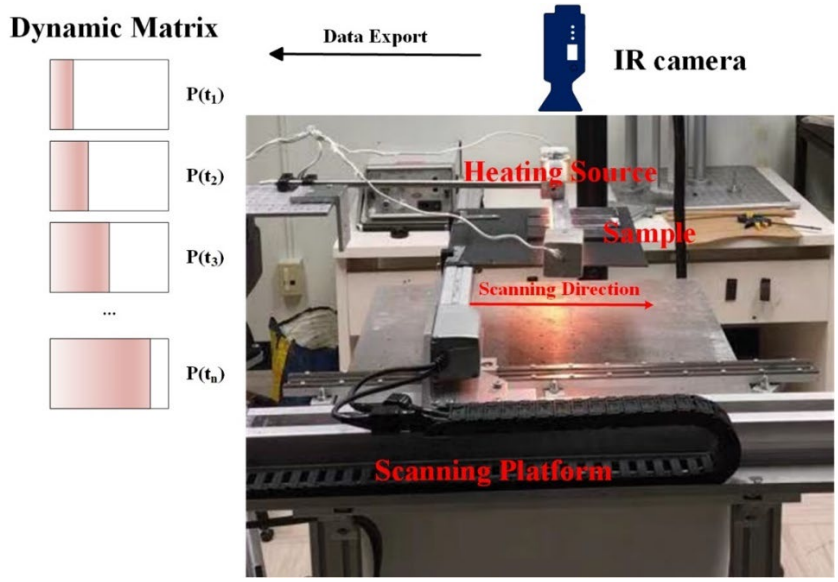


Fig. 2. Experimental setup for the line-scan active thermography.

In line-scan thermography, the temperature distribution in the direction normal to the surface from time equal to [-∞, t] can be expressed by [28]:

$$T(x,z,t) = \frac{q}{\pi k} \cdot e^{-\frac{v(x-vt)}{2\alpha}} \cdot K_0\left(\frac{v\sqrt{(x-vt)^2+L^2}}{2\alpha}\right) \tag{1}$$

where $K_0(x)$ is a modified Bessel function of the second kind of order zero, v is the movement velocity, L is the sample thickness, k is the thermal conductivity, α is the thermal diffusivity, and q is the rate of heat emitted per unit length.
Therefore, the temperature at the heated sample surface in line scan thermography can be expressed as:

$$T(x,t) = \frac{q}{\pi k} \cdot e^{-\frac{v(x-vt)}{2\alpha}} \cdot \left(K_0\left(\frac{v|x-vt|}{2\alpha}\right) + 2\sum_{n=1}^{\infty} K_0\left(\frac{v\sqrt{(x-vt)^2+(2nL)^2}}{2\alpha}\right)\right) \tag{2}$$

For a moving system, the surface temperature can be expressed as:

$$T(x) = \frac{q}{\pi k} \cdot e^{-\frac{vx}{2\alpha}} \cdot \left(K_0\left(\frac{v|x|}{2\alpha}\right) + 2\sum_{n=1}^{\infty} K_0\left(\frac{v\sqrt{x^2+(2nL)^2}}{2\alpha}\right)\right) \tag{3}$$

The terahertz imaging system is shown in Fig. 3. A pump beam and a reference beam are generated from the ultra-fast laser pulse. An optical time-delay line is used to time-shift the pump beam, which is then converted to a terahertz pulse using a terahertz emitter. A coupled detector catches the terahertz pulse as it passes through the sample. The sampling signal is the reference beam, which is implemented on the detector. After sampling, the terahertz signal is sent to a lock-in amplifier. The weak signal that has been amplified is analyzed during the data collection process.

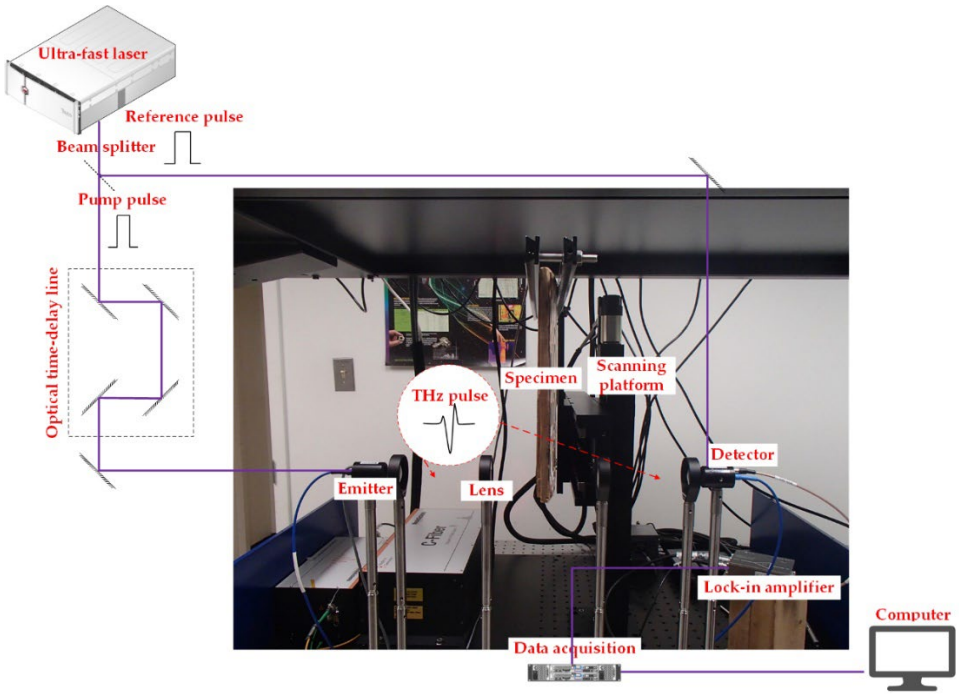


Fig. 3. The schematic diagram for the terahertz imaging system.

The terahertz time-domain spectroscopy (THz-TDS) system is manufactured by Menlo Systems GmbH, Munich, Germany. The system has a frequency resolution of 1.2 GHz, and a repetition rate of 100 MHz. The experiment is carried out in transmission mode. The scanning step is set at 0.5 mm.

As an extension of the FE-S-F framework [26], the fusion process is shown in Fig. 4. First of all, raw data from the active thermography and terahertz imaging systems is processed using feature extraction methods to gather features from temporal, frequency, and statistical aspects. Meanwhile, the SNR of each feature is calculated through the pixels sampled from both the defect region and the sound region [29]. Then, depending on the criterion of highest SNR, the best feature is selected for the fusion step. Finally, the selected features from two imaging systems are processed with cropping, rotating and scaling operators to maintain geometrical alignment, and then merged by an unsupervised deep residual network [30]; in this way, a fusion image including defect information from surface to interior of the sample can be realized.

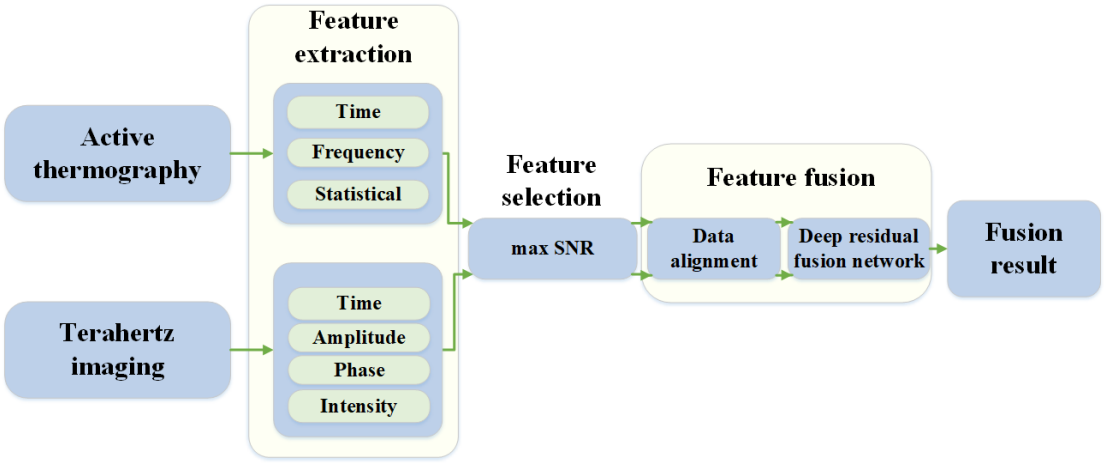


Fig. 4. The flowchart of the fusion technique.

In the feature extraction stage, data collected from both the active thermography and terahertz imaging can be regarded as a three-dimensional tensor $X \in R^{M\times N\times P}$, where M and N correspond respectively to the row and column of the tensor, whereas P refers to the number of time stamps in the data sequence. A time domain feature $X_{ij}(k)$ is just a typical frame extracted from the data sequence. Here, $i = 1,\ldots,M$ and $j = 1,\ldots,N$ jointly index the spatial location, and $k = 1,\ldots,P$ indexes the time stamp of the corresponding typical frame. The intensity of $X_{ij}(k)$ can be regarded as the maximum value of the transient response at each pixel, i.e.,

$$\text{intensity}_{ij} = \max(X_{ij}(k)) \tag{4}$$

where the $\max(\cdot)$ operator returns the maximal element of the length-P input vector.

In the feature selection stage, the SNR is calculated by taking 150 pixels from each defect region, alongside another 150 pixels from the sound area (i.e., a region with no defect). Mathematically, the SNR is given as:

$$\text{SNR} = 20\cdot\log_{10}\frac{\|X_d - X_s\|_1}{\sigma_s} \tag{5}$$

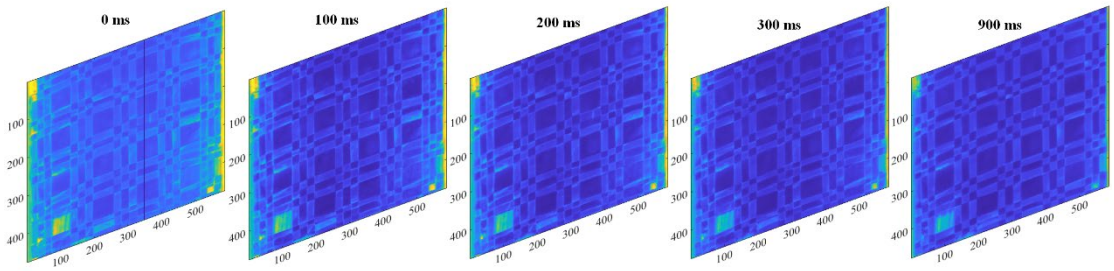
where X_d and X_s denote the vectors containing intensity values of the pixels from the defect and sound regions, respectively, and σ_s is the standard deviation, representing noise variability.

In the feature fusion stage, an unsupervised deep residual network is employed, of which the details on the network layers and architecture can be found in [31], and thus are not reiterated. In short, the network is modeled as an encoder–decoder architecture. The encoder contains a convolutional layer and a dense-connected block, which has the capacity to extract high-dimensional representations of feature images from different modalities. Then, these high-dimensional representations are fused with an l_1-norm based fusion rule and reconstructed by the decoder, which is composed of convolutional layers. The encoder combines dense connections with residual modules to extract high-dimensional representations from feature images. Residual learning can optimize several convolutional layers as identity mapping which eases the training of the deep neural network and, in parallel, benefits from increasing depth. Dense connections

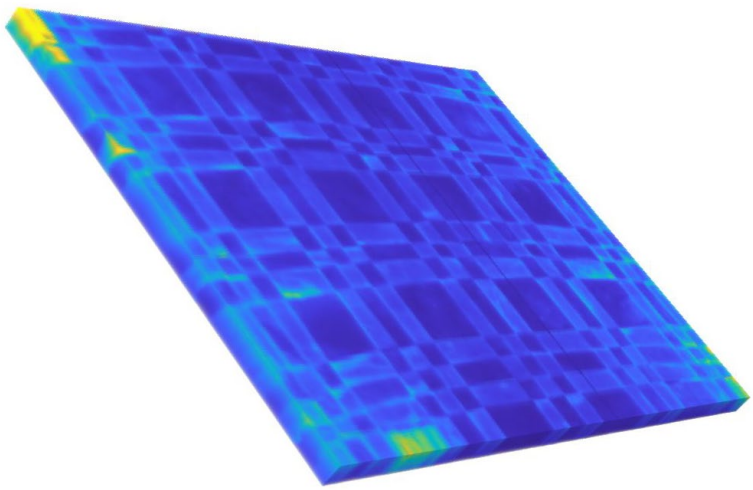
between residual blocks ensure that the input of each residual block is the concatenation of all of the former modules. This effectively protects the information in the middle layer from vanishing.

3 Results and discussion

The thermal sequence collected from the active thermography experiments is illustrated in Fig. 5. The cooling of surface temperature, see Fig. 5(a), is a result of the thermal diffusion process. It can be seen that the thermal contrast of some surface hot spots decreases gradually in time; these represent the scratches existing on the surface of the sample. Some regions with a higher thermal contrast do not change significantly over time; these regions correspond to defects of various kinds, namely, cracks, detachments, and the missing tesserae. According to the thermal diffusion theory from the surface to interior, a 3D reconstruction of the marquetry sample can be obtained from the thermal images acquired sequentially in time. The 3D reconstruction result is depicted in Fig. 5(b). It can be observed that the thermal contrast due to defect A, i.e., a missing tessera—recall Fig. 1(a)—persists along the "depth" (or z) direction, whereas the thermal contrast due to defect H, i.e., a broken tessera, only exists near the surface.



(a)



(b)

Fig. 5. Infrared thermography result of the ancient marquetry sample: (a) images of the different depths (from the surface to the internal layer of the sample), and (b) 3D reconstruction of the marquetry sample.

Fig. 6 shows the features of defect A extracted from the thermal image sequence. In this case, features include the time- and frequency-domain ones, as well as computed statistics. Time-domain feature refers to just the typical frames of thermal sequence. Frequency-domain features include amplitude feature and phase feature, which can be acquired from Fourier transform [32]. The amplitude feature is related to the surface of the sample up to a limited depth; it can be used to describe the surface morphological information. The phase feature is less sensitive to shape information, instead, it is linked to the depth reached by the thermal waves and thus allows calculation of defect depth. The first two statistical features are skewness and kurtosis, which are the third- and fourth-order standard central moments [33]. In addition to that, the first principal component calculated by principal component analysis (PCA) is used as another statistical feature [34]. From visual inspection, it is possible to conclude that time-domain, amplitude, and principal component features give higher contrast than others. Notwithstanding, phase, skewness and kurtosis features are more adequate in reflecting defects along the depth direction. This is shown in the stereo appearance of the defective area related to the missing tessera.

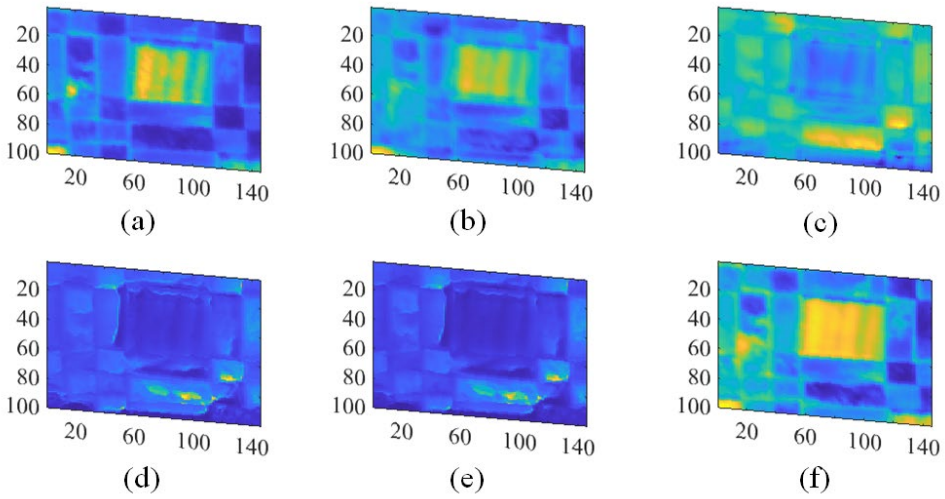


Fig. 6. Features of defect A extracted from infrared thermography sequence: (a) time-domain feature; (b) amplitude feature; (c) phase feature; (d) skewness feature; (e) kurtosis feature; and (f) principal component feature.

It should be noted that the selection of suitable features entering the fusion process cannot be based only on visual observation because any decision made thereof would have a sense of subjectivity attached to it, for that reason, the authors consider the SNR of the defective area as the criterion for feature selection. More particularly, the feature that has the highest SNR is to be selected for the fusion process. To demonstrate the SNR-based feature selection, the SNR of each feature is calculated for two missing tesserae (defects A and E) and one detachment (defect F). Recall Eq. (5), in that, X_d for each defect is a vector of 150 pixels surrounding that defect, whereas X_s, in all three cases, is a vector of 150 sound-area pixels in the neighborhood of defect A. Since there are three defects of interest and six features, a total of 18 SNR values are computed and

shown in Fig. 7. It can be observed that the time-domain feature has the highest SNR. Amplitude feature and principal component feature also shown interesting thermal contrasts, as evidenced from the high SNR. These observations are consistent with the visual representations in Fig. 6.

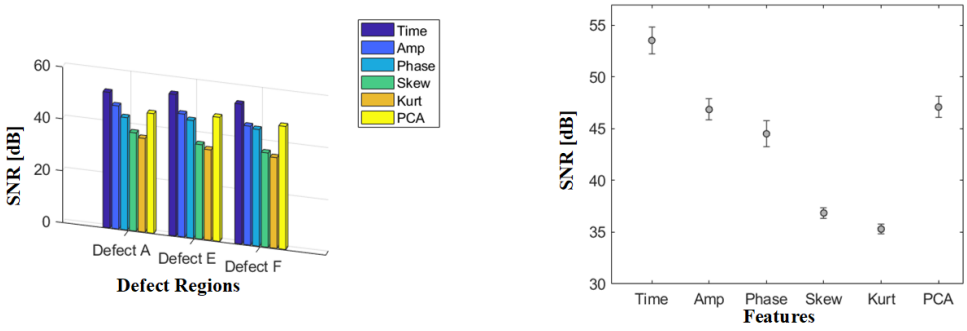


Fig.7. SNR calculated for feature selection. (a) SNR on the defective region of each feature, and (b) average SNR of each feature.

Fig. 8 illustrates the terahertz time-domain spectroscopy analysis on the marquetry sample. The experiment is carried out in the transmission mode. Therefore, the intensity of each point shows the attenuation of terahertz wave in the marquetry. As visible from the left panel of Fig. 8, the areas related to the missing tesserae have higher intensities than other regions; this is true especially for the regions of defects A, B and E, cf. Fig. 1. It should be noted that the area along the left boundary of the sample has a lower thickness than other areas, which can also be seen from the rear side photo shown in Fig. 1(b). This leads to a lower signal attenuation of the terahertz waves, corresponding to a higher intensity. Another interesting point is related to the damaged part on the rear side of the sample, behind defect D, see Figs. 1(a) and 1(b). This part shows a higher attenuation of the terahertz signal as visible in the related image. The possible reason can be linked to the fact that the decay of the fir wood leads to alternation of its thermal properties.

With the aim of performing spectroscopic analyses on this sample, the present authors select and put to analysis some image pixels from the defective regions. Time and frequency domain curves are generated accordingly. As shown in the time-domain curve (Fig. 8), the main peak of terahertz wave detected on the missing tesserae (i.e., defects A and B) arrived earlier than the one detected on the detached region (defect G). Due to the absence of the tesserae, the thickness of the sample (considering the terahertz wave propagation path) is reduced, which results in the shorter time delay of the peak arrival on these regions. On the other hand, it is possible to see in the spectrum that the region with tesserae has higher attenuation than the missing tesserae regions.

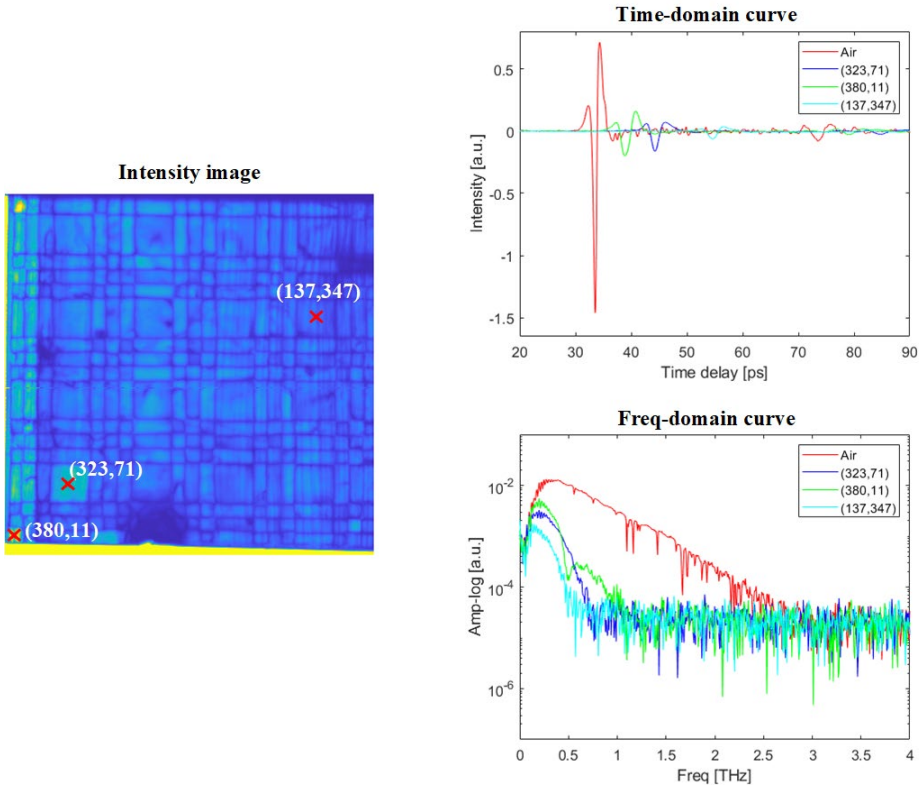


Fig. 8. Terahertz time and frequency domain analysis on the marquetry sample.

Considering that terahertz imaging needs to provide internal defect information to complement the active thermography imaging, more attention during the feature extraction and selection process of terahertz imaging ought to be paid to the area of interior defects such as detachments. Shown in Fig. 9 are features of defect G region extracted from terahertz imaging system, which include time-domain, intensity, amplitude and phase features. Its time-domain feature is chosen at the arrival time (56.63 ps) of the main peak. However, time-domain feature only contains information about the detachment area. Other detailed information such as the location of inlays is missing from this feature. The intensity feature and amplitude feature both show the attenuation of terahertz wave in different materials. The intensity feature, i.e., Fig. 9(b), is recorded point-by-point as the highest peak value of the time-domain curve. Besides, the amplitude feature is calculated based on the frequency-domain curve. As is well known, the physical properties especially the absorption coefficient are affected by frequency, which also leads to the variation of attenuation in the spectrum. As shown by the frequency-domain curves in Fig. 8, the amplitudes of different materials have noticeable differences at 0.56 THz. Therefore, this frequency point is chosen to obtain the amplitude feature, as shown in Fig. 9(c). Comparing these two features focusing on the attenuation, it can be concluded that the intensity feature has higher contrast at the boundaries of the tesserae, whereas the phase feature is sensitive to the variation along the depth direction, which has led to the high contrast over the detachment region. It is worth noting that, as compared to time-domain feature, phase feature preserves more details on the location and shape of tesserae. This can complement the contrast suppression on the feature from active thermography during the fusion process. The SNR shown in Table 1 is calculated on the basis of defect G. Then, on the basis of the

highest SNR criterion, phase feature of terahertz imaging is selected for the fusion process.

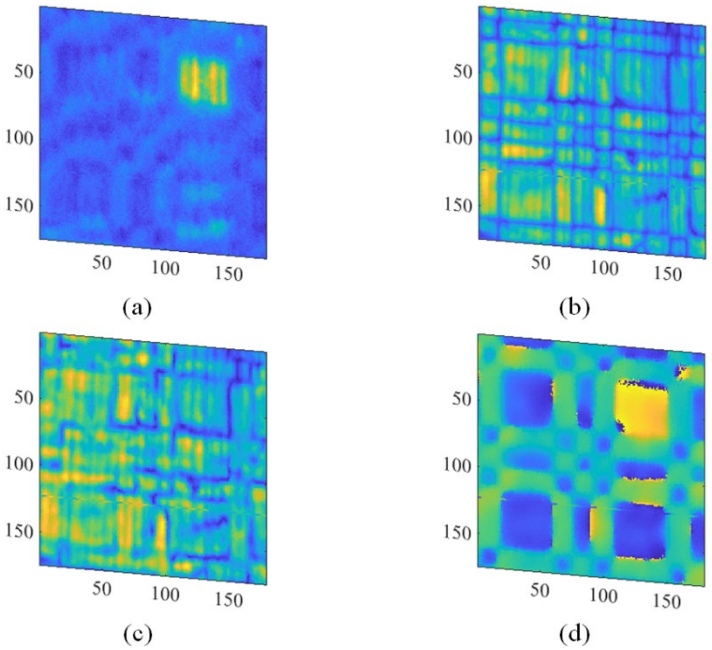


Fig. 9. Features of defect G area extracted from terahertz imaging system: (a) time-domain feature; (b) intensity feature; (c) amplitude feature; and (d) phase feature.

Table 1. SNR calculated for feature selection on defect G.

Time feature	Intensity feature	Amplitude feature	Phase feature
49.52	42.95	42.00	59.24

Fig. 10 illustrates the final fusion results. The fusion technique is able to successfully detect all defects, with high contrast, such as the missing tesserae A, B, C, E and the defects F, G (detachments). It is worth mentioning that, the deep detachment G cannot be retrieve by active thermography alone. This part has been integrated by fusing the feature image provided by terahertz imaging. In addition, the defects due to the decay in support layer have also been detected in the final result. Active thermography provides useful surface information such as the shapes of the tesserae or scratches (see region 2 and 3, for reference). Terahertz imaging gathers internal defects and material distribution information. The fusion technique extended from FE-S-F framework extracts features containing high-contrast defect information; these features have been integrated into the final fusion image, showing defect information at different depths.

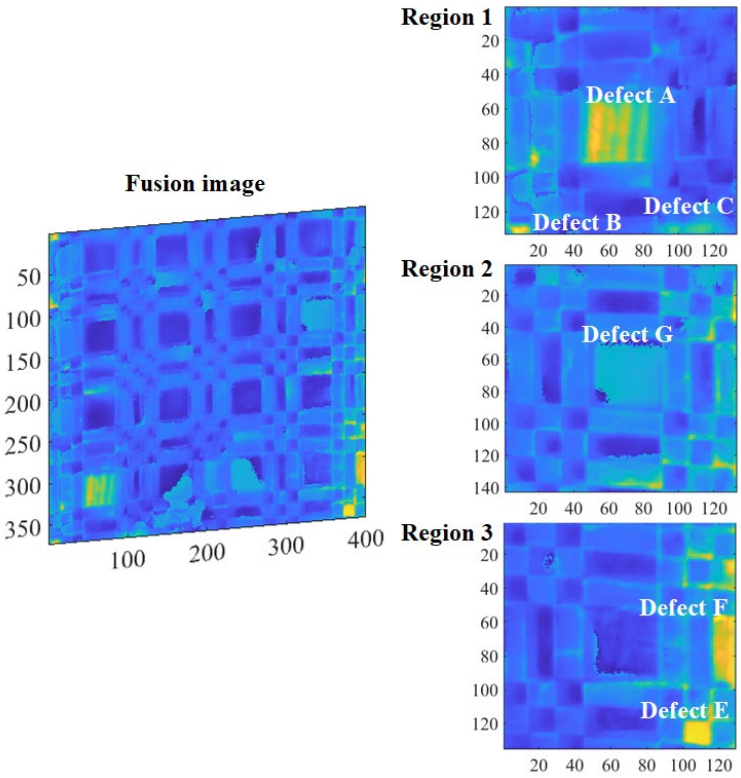


Fig. 10. Fusion result on marquetry sample (left), alongside three zoomed insets over some specific regions (right).

4 Conclusion

In this work, a non-invasive fusion imaging method has been investigated and proven capable of being used for cultural heritage inspection. An ancient marquetry with natural defects has been inspected via line-scan thermography and terahertz imaging systems. To integrate the morphological information provided by active thermography and internal material information collected from terahertz imaging, a fusion method is developed based upon the feature extraction, selection and fusion framework. Time-domain, frequency-domain and statistical features are selected based on the signal-to-noise ratio (SNR) of the defective region and, finally, fused by an unsupervised deep residual fusion network.

The non-invasive fusion imaging method successfully reveals the defects such as missing tesserae or splitting located at different depths. The experiment has demonstrated that the proposed fusion imaging has the potential to provide high SNR defect information and high thermal contrast results for the cultural heritage inspection. This complementarity must be commended. Finally, the combination of terahertz stratigraphic imaging, which can provide images at different depths, and 3D extension of the fusion imaging are to be further investigated on other materials [35], [36].

Acknowledgements

This work is supported by the Canada Research Chair in Multipolar Infrared Vision (MiViM), the Natural Sciences and Engineering Research Council (NSERC) of Canada through the Discovery Grant program and the Create-oN DuTy! program.

This work is also supported by the National Key Laboratory of Science and Technology on Advanced Composites in Special Environments through Open-end Research Fund program, and the National Natural Science Foundation of China under Grant No.61902220.

References

[1] A. Obrutsky, D. Acosta, A. Garcia, and J. Scopelliti, "Non-destructive testing methods used for the study of cultural heritage in Argentina," *Insight-Non-Destructive Test. Cond. Monit.*, vol. 51, no. 9, pp. 499–503, 2009.

[2] I. Garrido, S. Lagüela, S. Sfarra, and P. Arias, "Development of thermal principles for the automation of the thermographic monitoring of cultural heritage," *Sensors*, vol. 20, no. 12, p. 3392, 2020.

[3] I. Garrido *et al.*, "Introduction of deep learning in thermographic monitoring of cultural heritage and improvement by automatic thermogram pre-processing algorithms," *Sensors*, vol. 21, no. 3, p. 750, 2021.

[4] G. Bitossi, R. Giorgi, M. Mauro, B. Salvadori, and L. Dei, "Spectroscopic techniques in cultural heritage conservation: a survey," *Appl. Spectrosc. Rev.*, vol. 40, no. 3, pp. 187–228, 2005.

[5] L. Lanteri, G. Agresti, and C. Pelosi, "A new practical approach for 3D documentation in ultraviolet fluorescence and infrared reflectography of polychromatic sculptures as fundamental step in restoration," *Heritage*, vol. 2, no. 1, pp. 207–215, 2019.

[6] S. Dos Santos, M. Lints, N. Poirot, and A. Salupere, "Optimized excitation for nonlinear wave propagation in complex media: From biomedical acoustic imaging to nondestructive testing of cultural heritage," *J. Acoust. Soc. Am.*, vol. 138, no. 3, p. 1796, 2015.

[7] H. Fernandes *et al.*, "Characterization of Ancient Marquetry Using Different Non-Destructive Testing Techniques," *Appl. Sci.*, vol. 11, no. 17, p. 7979, 2021.

[8] A. O. Chulkov *et al.*, "Evaluating quality of marquetries by applying active IR thermography and advanced signal processing," *J. Therm. Anal. Calorim.*, vol. 143, no. 5, pp. 3835–3848, 2021.

[9] Y. Duan *et al.*, "Automated defect classification in infrared thermography based on a neural network," *NDT \& E Int.*, vol. 107, p. 102147, 2019.

[10] C. Hu *et al.*, "LSTM-RNN-based defect classification in honeycomb structures using infrared thermography," *Infrared Phys. \& Technol.*, vol. 102, p. 103032, 2019.

[11] F. Wang *et al.*, "Quantitative non-destructive evaluation of CFRP delamination defect using laser induced chirp-pulsed radar photothermal tomography," *Opt.*

Lasers Eng., vol. 149, p. 106830, 2022.
[12] X. Lu, H. Sun, T. Chang, J. Zhang, and H.--L. Cui, “Terahertz detection of porosity and porous microstructure in pharmaceutical tablets: A review,” *Int. J. Pharm.*, vol. 591, p. 120006, 2020.
[13] T. Chang, X. Zhang, Q. Guo, Y. Li, L. Liu, and H.-L. Cui, “Terahertz dielectric spectroscopy based thermal aging analysis of polypropylene,” *IEEE Trans. Terahertz Sci. Technol.*, vol. 10, no. 4, pp. 363–369, 2020.
[14] J. Wang *et al.*, “Nondestructive damage evaluation of composites based on terahertz and X-ray image fusion,” *NDT \& E Int.*, p. 102616, 2022.
[15] E. Grinzato, P. G. Bison, and S. Marinetti, “Monitoring of ancient buildings by the thermal method,” *J. Cult. Herit.*, vol. 3, no. 1, pp. 21–29, 2002.
[16] N. P. Avdelidis and A. Moropoulou, “Applications of infrared thermography for the investigation of historic structures,” *J. Cult. Herit.*, vol. 5, no. 1, pp. 119–127, 2004.
[17] P. Theodorakeas, N. P. Avdelidis, E. Cheilakou, and M. Koui, “Quantitative analysis of plastered mosaics by means of active infrared thermography,” *Constr. Build. Mater.*, vol. 73, pp. 417–425, 2014.
[18] P. Theodorakeas *et al.*, “NDT inspection of plastered mosaics by means of transient thermography and holographic interferometry,” *NDT \& E Int.*, vol. 47, pp. 150–156, 2012.
[19] F. Mercuri *et al.*, “Combined use of infrared imaging techniques for the study of underlying features in the Santa Maria in Cosmedin altarpiece,” *Archaeometry*, vol. 63, no. 5, pp. 1009–1023, 2021.
[20] P. Tavakolian, S. Sfarra, G. Gargiulo, K. Sivagurunathan, and A. Mandelis, “Photothermal coherence tomography for 3-D visualization and structural non-destructive imaging of a wood inlay,” *Infrared Phys. \& Technol.*, vol. 91, pp. 206–213, 2018.
[21] Y. Yao *et al.*, “Active thermography testing and data analysis for the state of conservation of panel paintings,” *Int. J. Therm. Sci.*, vol. 126, pp. 143–151, 2018.
[22] J. B. Jackson *et al.*, “A survey of terahertz applications in cultural heritage conservation science,” *IEEE Trans. Terahertz Sci. Technol.*, vol. 1, no. 1, pp. 220–231, 2011.
[23] R. M. Groves, B. Pradarutti, E. Kouloumpi, W. Osten, and G. Notni, “2D and 3D non-destructive evaluation of a wooden panel painting using shearography and terahertz imaging,” *Ndt E Int.*, vol. 42, no. 6, pp. 543–549, 2009.
[24] J. Dong *et al.*, “Terahertz frequency-wavelet domain deconvolution for stratigraphic and subsurface investigation of art painting,” *Opt. Express*, vol. 24, no. 23, pp. 26972–26985, 2016.
[25] Z. Liu, D. S. Forsyth, J. P. Komorowski, K. Hanasaki, and T. Kirubarajan, “Survey: State of the art in NDE data fusion techniques,” *IEEE Trans. Instrum. Meas.*, vol. 56, no. 6, pp. 2435–2451, 2007.
[26] J. Hu *et al.*, “Multi-Excitation Infrared Fusion for Impact Evaluation of Aluminium-BFRP/GFRP Hybrid Composites,” *Sensors*, vol. 21, no. 17, p.

5961, 2021.
[27] C.-M. Wen, S. Sfarra, G. Gargiulo, and Y. Yao, “Thermographic data analysis for defect detection by imposing spatial connectivity and sparsity constraints in principal component thermography,” *IEEE Trans. Ind. Informatics*, vol. 17, no. 6, pp. 3901–3909, 2020.
[28] H. Zhang, S. Sfarra, C. Ibarra-Castanedo, and X. P. V Maldague, “Dynamic Line-Scan Thermography for the Inspection of Paper-Based Materials: A Case Study Focused on an Ancient Book Cover,” in *Multidisciplinary Digital Publishing Institute Proceedings*, 2019, vol. 27, no. 1, p. 9.
[29] H. Zhang *et al.*, “An infrared-induced terahertz imaging modality for foreign object detection in a lightweight honeycomb composite structure,” *IEEE Trans. Ind. Informatics*, vol. 14, no. 12, pp. 5629–5636, 2018.
[30] J. Hu, H. Zhang, S. Sfarra, C. Santulli, and X. Maldague, “Three-Dimensional Non-Destructive Inspection Using Novel Infrared-Terahertz Fusion Approaches,” *Eng. Proc.*, vol. 8, no. 1, p. 24, 2021.
[31] J. Hu, H. Zhang, S. Sfarra, C. Santulli, G. Tian, and X. Maldague, “Novel infrared-terahertz fusion 3D non-invasive imaging of plant fibre-reinforced polymer composites,” *Compos. Sci. Technol.*, p. 109526, 2022.
[32] X. Maldague, F. Galmiche, and A. Ziadi, “Advances in pulsed phase thermography,” *Infrared Phys. Technol.*, vol. 43, no. 3–5, pp. 175–181, 2002.
[33] F. J. Madruga, C. Ibarra-Castanedo, O. M. Conde, J. M. López-Higuera, and X. Maldague, “Infrared thermography processing based on higher-order statistics,” *NDT E Int.*, vol. 43, no. 8, pp. 661–666, 2010.
[34] N. Rajic, “Principal component thermography for flaw contrast enhancement and flaw depth characterisation in composite structures,” *Compos. Struct.*, vol. 58, no. 4, pp. 521–528, 2002.
[35] N. Tao, C. Wang, C. Zhang, and J. Sun, “Quantitative measurement of cast metal relics by pulsed thermal imaging,” *Quant. Infrared Thermogr. J.*, vol. 19, no. 1, pp. 27–40, 2022.
[36] K. Liu, K.-L. Huang, S. Sfarra, J. Yang, Y. Liu, and Y. Yao, “Factor analysis thermography for defect detection of panel paintings,” *Quant. Infrared Thermogr. J.*, pp. 1–13, 2022.

DSPACE

https://dspace.org/

Non-destructive imaging of marqueteries based on a new infrared-terahertz fusion technique

Hu, Jue; Zhang, Hai; Sfarra, Stefano; Gargiulo, Gianfranco; Avdelidis, Nicolas P. ...

2022-06-29
Elsevier
https://doi.org/10.1016/j.infrared.2022.104277
Hu J, Zhang H, Sfarra S, et al., (2022) Non-destructive imaging of marqueteries based on a new infrared-terahertz fusion technique. Infrared Physics and Technology, Volume 125, September 2022, Article number 104277

Downloaded from a DSpace repository. https://dspace.org/